

# Consistency of Implicit and Explicit Features Matters for Monocular 3D Object Detection

Qian Ye, Ling Jiang, Yuyang Du

DiDi

Beijing, China

{noahye, jiangling, duyuyang}@didiglobal.com

## Abstract

*Monocular 3D object detection is a common solution for low-cost autonomous agents to perceive their surrounding environment. Monocular detection has progressed into two categories: (1) Direct methods that infer 3D bounding boxes directly from a frontal-view image; (2) 3D intermedia representation methods that map image features to 3D space for subsequent 3D detection. The second category is standing out not only because 3D detection forges ahead at the mercy of more meaningful and representative features, but because of emerging SOTA end-to-end prediction and planning paradigms that require a bird's-eye-view feature map from a perception pipeline. However, in transforming to 3D representation, these methods do not guarantee that objects' implicit orientations and locations in latent space are consistent with those explicitly observed in Euclidean space, which will hurt model performance. Hence, we argue that consistency of implicit and explicit features matters and present a novel monocular detection method, named **CIEF**, with the first orientation-aware image backbone to eliminate the disparity of implicit and explicit features in subsequent 3D representation. As a second contribution, we introduce a ray attention mechanism. In contrast to previous methods that repeat features along the projection ray or rely on another intermedia frustum point cloud, we directly transform image features to voxel representations with well-localized features. We also propose a hand-crafted gaussian positional encoding function that outperforms the sinusoidal encoding function but maintains the benefit of being continuous. **CIEF** ranked 1st among all reported methods on both 3D and BEV detection benchmark of KITTI at submission time.*

## 1. Introduction

Monocular 3D object detection is widely used in driving automation systems and advanced driver-assistance system

to perceive external environment. An object is detected in a monocular setting means that its location, size and orientation are estimated from an image captured by one camera. Despite the fact that most vehicles are equipped with multiple cameras, monocular object detection remains indispensable, as many areas are visible to only one camera. Detected objects, such as cars, pedestrians, and traffic lights, will be used by vehicles to perform dynamic driving tasks, like crash avoidance and adaptive cruise control.

The performance of monocular 3D object detection leaps forward by operating not only on a frontal-view image plane but also on a 3D space that gathers projected image features [18, 23, 26, 27, 35]. An intermedia 3D scene representation has an inherent advantage that euclidean distance of its coordinate system are more meaningful and scales of objects are depth-independent [23, 26, 27]. On the other hand, more and more of SOTA end-to-end prediction and planning paradigms require bird's-eye-view feature map from a perception pipeline as input.

Existing works typically use camera extrinsic together with pixel depth estimated by image-based network to transform features from 2D image plane to 3D space. However, by directly feeding RGB value or raw feature from canonical 2D image backbone to 3D space, they all neglect or limit the power of the 2D image backbone. In the first case, the backbone of the image functions as a depth estimator that, except for pixels' depths, does not contribute anything to 3D representation. The second case does not ensure that features implicitly embedded by the projected feature vectors are consistent with that explicitly represented in Euclidean space. For example, the orientation of an object observed in image, who is subsequently transformed to an implicit information in a feature vector by image backbone, might conflict with the orientation macroscopically observed in Euclidean space. This is because mounting error of camera and the need of 3D world rotation augmentation [23, 37] result in relative orientation variance between camera coordinate and the ego-car coordinate. Thus, following 3D network (e.g., 3D or bird's-eye-view convolu-

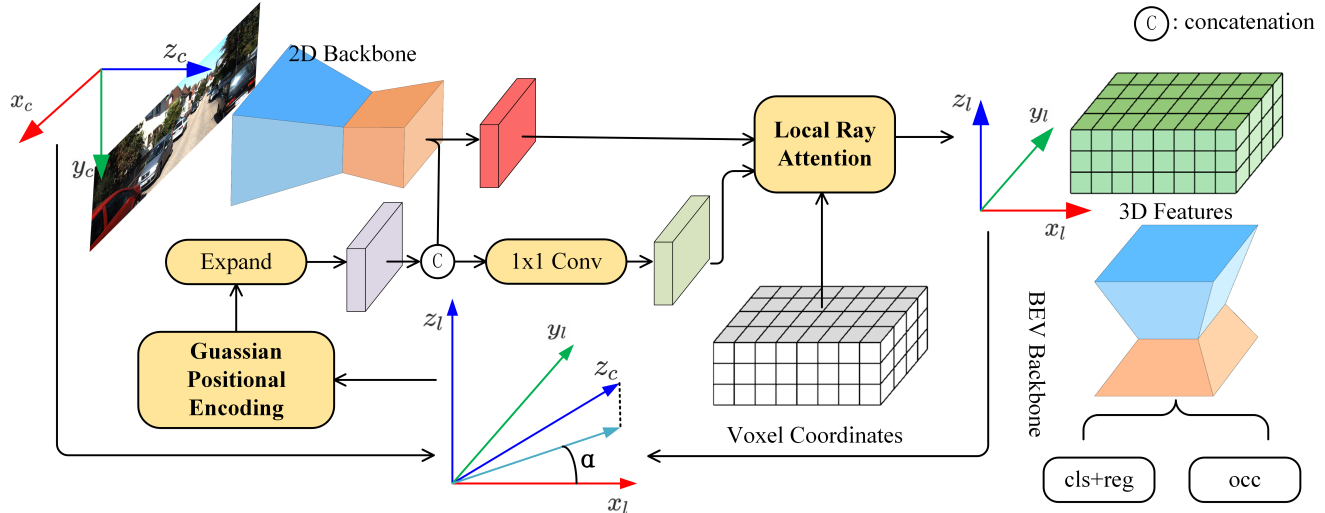


Figure 1. Overall Architecture.

tion, PointNet [24]) will receive conflict information.

We argue that there should be no conflict between implicit features in latent space and explicit features in Euclidean space, where the latent space is constituted by all possible vectors of a particular point or voxel in 3D representation. Motivated by this insight, we propose a novel end-to-end orientation-aware detection system that bridge the gap between 2D and 3D representation.

The main contribution of our work are as follows:

1. We present the first orientation-aware image backbone to eliminate the disparity between implicit and explicit orientations of objects in 3D representation.
2. We introduce a ray attention mechanism that efficiently and directly transforms image-view features to voxel representations.
3. We propose a handcrafted gaussian positional encoding function that outperforms the sinusoidal positional encoding function but maintain the benefit of being continuous.

Experiments in the KITTI object detection benchmark show that our model achieves top results in two challenging tasks (ranked 1st on the BEV benchmark and 1st on the 3D benchmark).

## 2. Related Work

### 2.1. Direct Methods based on A Frontal View

Without extra data, such as depth maps, CAD models, standard monocular detectors use only a single frontal-view image as input and infer 3D bounding boxes from grids in the image plane. Previous 3D object detection

methods mostly follow 2D detection methods, which directly predict 3D bounding boxes without predicting an intermediate 3D scene representation. With cues from object shapes and scene geometry, these methods can incorporate the geometric relation between the 2D image plane and 3D space. SMOKE [16] removes 2D detection network and propose concise architectures for 3D detection built on CenterNet [39]. FCOS3D [32] extends the 2D detector FCOS [30] by adding heads that predict various 3D cuboid parameterizations. MonoCon [15] adds auxiliary context regression heads to assist 3D detection. DETR3D [33], based on DETR, uses transformer for end-to-end 3D bounding box prediction by projecting learnable 3D queries in 2D images. MonoDTR [9] learns depth information by depth-aware transformer. To further strengthen the detection accuracy, recent methods have introduced geometric priors into the networks. MonoPair [1] leverage geometric consistency between adjacent object pairs, formulating the inference as a constrained optimization problem with uncertainty. Pseudo-Stereo-3D [19] propose a Pseudo-Stereo 3D detection framework, which generates a virtual view, for monocular 3D detection. These methods only produce sparse depth for every target, which lead to fewer hyper-parameters. However, due to the lack of depth information, these methods often are accurate only in close vicinity and fail to accurately localize objects. In order to effectively leverage large-scale depth data, DD3D [20] adds a depth prediction head for pre-training and generate depth values for every pixel in an image. MonoDDE [12] proposes a depth solving system produces 20 diverse depths in different ways to avoid depth assumption failure in other ways. However, multiple voxels can be projected to the same pixels on 2D plane independent of the depth of the object at that pixel, on which the same object has different scales leading

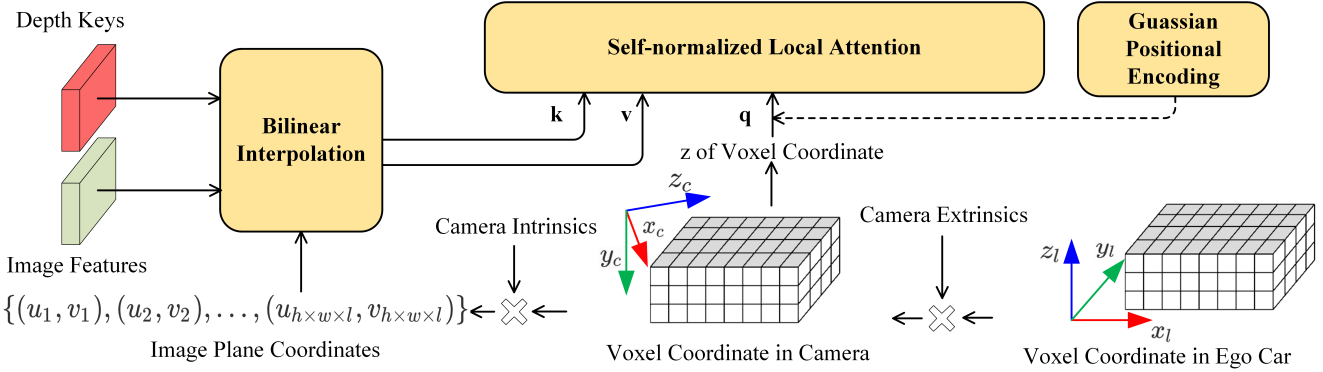


Figure 2. Illustration of local ray attention mechanism.

to reduced detection accuracy.

## 2.2. 3D Intermedia Representation Methods

Representing feature in 3D space, such as bird’s eye view representations or Pseudo-LiDAR representations, overcome the limitations of perspective range view, e.g. occlusion or variability in scale. Methods transform image features into bird’s eye view features with the depth information from depth estimation or categorical depth distribution. OFT [27] introduces an orthographic feature transform to project a fixed cube of voxels onto image features to generate the bird’s eye view representation of the scene. Lift-Splat [23] learns categorical depth distributions in an unsupervised manner to generates the bird’s eye view representations. With the trend of transformer, BEVFormer [13] learning bird’s eye view representation from multi-camera images via spatiotemporal transformers to capture information across cameras. Bird’s eye view based method which is based on depth information is sensitive to the accuracy of depth information. The detection performance of bird’s eye view based methods achieve limited performance caused by inaccurate depth priors. Image features can also be converted to 3D point clouds, commonly known as Pseudo-LiDAR, by leveraging depth information and calibration parameters. CaDDN [26] predicts categorical depth distributions for each pixel to construct Pseudo-LiDAR representations and applies a LiDAR-based 3D detector to predict 3D bounding boxes. Mono3DPLiDAR [35] use bounding box consistency constraint to mitigate the local misalignment and long tail issues in the noisy pseudo-LiDAR. Ma et al. [18] transform 2D image plane to Pseudo-LiDAR and embed the complementary RGB cue into the generated point clouds representation. BEVDet [8] learning Pseudo-LiDAR representation from multi-camera images to performs 3D object detection. LPCG [21] using LiDAR point clouds to generate massive 3D box pseudo labels for monocular methods. However, the performance of these methods rely on the accuracy of image-to-LiDAR gener-

ation, which has a huge gap between Pseudo-LiDAR and LiDAR-based detectors.

## 3. Method

### 3.1. Overview

As illustrated in Figure 1, our work is composed of a 2D image backbone, local ray attention, a BEV backbone and a feedback loop that informs the 2D backbone orientation differences of objects between the image and the bird’s-eye view in Euclidean space.

Given a single image captured by a color camera mounted on top of a vehicle, the 2D backbone produces two feature maps namely depth keys and image features. The orientation differences encoded by the gaussian positional encoding method are then expanded to the same size as the image features. We concatenated the image features with the expanded orientation differences to produce the image values. The depth keys, image values, and voxel coordinates are fed to local ray attention to produce 3D representation. A BEV backbone processes the 3D representation and predicts 3D bounding boxes and a 3D occupancy map.

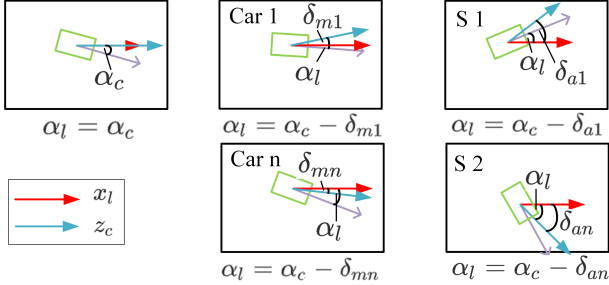
### 3.2. Local Ray Attention

Local ray attention directly transforms feature map of image to 3D voxel features without intermedia pseudo lidar representation (see Figure 2). Benefit from the attention mechanism, this process can adaptively place 2D features in proper 3D locations.

The inputs are depth keys and image features from the 2D backbone, and center coordinates of voxels obtained by evenly dividing a pre-defined detection area. Timing camera extrinsic, voxel center coordinates are transformed from ego-car coordinate system to camera coordinate system. Given camera intrinsic, we further get pixel coordinates of every voxel center by projecting them to the image plane. Bilinearly interpolating depth keys and image features at the projected pixel coordinate respectively pro-



(a) An image captured.



(b) Different cases from a bird's-eye-view perspective.

Figure 3. Variance of orientation observed from bird's-eye view in Euclidean space.

duces keys and values to self-normalized local attention. The  $z$  of voxel center coordinate in camera coordinate system are embedded by gaussian positional encoding function as a query.

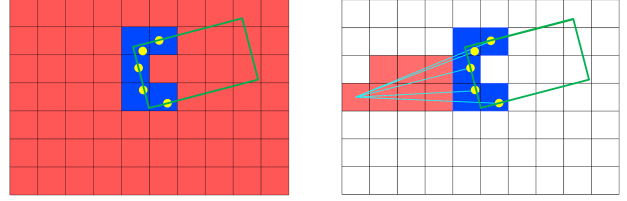
Given keys, values, and queries, the self-normalizing local attention firstly back projects the keys and values to their corresponding voxels. Every voxel is populated with a value weighted by the similarity between its query and the key.

$$\vec{v} = \text{sim}(\vec{p}, \vec{d})\vec{v} \quad (1)$$

### 3.3. Orientation-Aware 2D Image Backbone and Augmentation

After transforming features from the frontal-view image plane to the 3D space, the explicit orientation observed in Euclidean space may vary as shown in Figure 3. Ideally, the camera coordinate should be consistent with the ego-car coordinate (first column of Fig. 3b), which is impossible in practice due to the mounting error of the camera (the second column of Fig. 3b). The ego-car coordinate of each car will have a different offset of rotation. Moreover, during the training process, to prevent the BEV backbone from overfitting, data augmentation (i.e. randomly world rotation) is applied to the 3D representation leading to a large deviation in target orientation (the third column of Fig. 3b).

To solve this problem, we propose an orientation-aware image backbone. After data augmentation, we get the ego car coordinate system, axes with which the edges of 3D voxels are aligned. Suppose  $z'_c$  is the projection of the  $z_c$  axis in the  $x_l - y_l$  plane, we calculate orientation differences  $\delta$  of  $z'_c$  and  $x_l$  with camera extrinsic.  $\delta$  is then encoded by handcrafted gaussian positional encoding to get the vector



(a) Taking voxel without point as empty space results in false negative.

(b) Only voxels passed through by the laser rays must be true negative.

Figure 4. An example of a slice of occupancy map at a certain height. For demonstration purposes, voxel sizes and bounding boxes are adjusted from their real settings.

representation of  $\delta$ ,  $p_\delta$ . We do not perform instance augmentation [8, 37], that is, the orientation offset is the same for all locations. Hence,  $p_\delta$  is simply expanded to the same size as image features and concatenated with it. Following a layer of 1x1 convolution, image features that is implicitly consistent with the explicit features is obtained.

Data augmentation will affect the consistency as aforementioned, so the deployed augmentation strategy is discussed here. We use random world flipping of images and random world rotation augmentation. For random world flipping, ground truth bounding boxes, image, and the camera coordinate flip around the x-axis of ego-car coordinate. For random world rotation, we rotate the ego-car coordinate with the others remaining unchanged.

### 3.4. Handcrafted Gaussian Positional Encoding

In attention mechanism, positional encodings or linearly transformed positional encodings are widely adopted to provide their cosine similarity as a portion of attention weight to gather values [2, 25]. If the distance between two positions is observed with random fluctuating noise, we assume that ideally, the probability density of observed distances between two actually same positions must obey univariate normal distribution.

#### Definition

We define a probability density function:

$$f(x, \mu) = \frac{1}{\sqrt{\pi}\sigma} e^{-\frac{(x-\mu)^2}{\sigma^2}} \quad (2)$$

We define our positional encoding function  $g(d)$  which transforms position  $d \in [d_{min}, d_{max}]$  to a vector.

$$g(d) = [f(x_1, d)\Delta x, \dots, f(x_n, d)\Delta x] \quad (3)$$

where  $\{x_1, \dots, x_n\}$  is a set of  $n$  uniformly spaced points over an interval  $[x_0, x_n]$ ,  $x_0 \gg d_{min}$  and  $x_n \ll d_{max}$ .

#### Claim

Method	3D AP@0.7			BEV AP@0.7		
	Easy	Mod.	Hard	Easy	Mod.	Hard
OFT-Net [27]	2.50	3.28	2.27	9.50	7.99	7.51
CaDDN [26]	19.17	13.41	11.46	27.94	18.91	17.19
AM3D [18]	21.48	16.08	15.26	N/A	N/A	N/A
MonoDTR [9]	21.99	15.39	12.73	28.59	20.38	17.14
MonoDETR [38]	24.52	16.26	13.93	32.20	21.45	18.68
MonoCon [15]	22.50	16.46	13.95	31.12	22.10	19.00
DD3D [20]	23.19	16.87	14.36	32.35	23.41	20.42
MonoDDE [12]	24.93	17.14	15.10	33.58	23.46	20.37
GCDR+DDA [7]	25.21	17.25	13.53	37.86	27.92	21.97
PS-fld [19]	23.74	17.74	15.14	32.64	23.76	20.64
LPCG-Monoflex [21]	25.56	17.80	15.38	35.96	24.81	21.86
MonoInsight [6]	27.71	19.04	16.03	34.85	24.23	20.87
<b>CIEF (Ours)</b>	<b>31.55</b>	<b>20.95</b>	<b>17.83</b>	<b>41.41</b>	<b>28.50</b>	<b>23.88</b>
LPCG + DM3D [22]	<i>29.15</i>	<i>21.24</i>	<i>19.18</i>	<i>39.74</i>	<i>28.84</i>	<i>26.08</i>
<b>CIEF + DM3D (Ours)</b>	<b>35.96</b>	<b>25.02</b>	<b>21.47</b>	<b>46.17</b>	<b>33.13</b>	<b>28.80</b>

Table 1. Object detection results for car category ( $AP|_{R_{40}}$  metric [28]) on the KITTI [4] test set. Our model outperforms all previously published state-of-the-art one-stage and pseudo-lidar methods in both 3D and BEV benchmarks for all difficulty levels. The best results are marked in bold and the second best results are in italics. DM3D [22] though not practical for autonomous robots by just producing more boxes to increase recall, improves AP significantly. For a fair comparison, we also report DM3D applied to our model verse the best model in its original paper, LPCG + DM3D [22]. Our results are still the best for all metrics.

For  $\Delta d$  with its probability density function defined as the cosine similarity of  $g(d_1)$  and  $g(d_2)$  (see Equation (4)),  $\Delta d \sim \mathcal{N}(0; \sigma)$ .

$$P(\Delta d) = g(d_1) \cdot g(d_2) \quad (4)$$

**Proof**

$$\begin{aligned} P(\Delta d) &= g(d_1) \cdot g(d_2) \\ &\approx \int_{-\infty}^{+\infty} f(x, d_1) \cdot f(x, d_2) dx \quad (5) \\ &= \frac{1}{\sigma\sqrt{2\pi}} e^{-\frac{\Delta d^2}{2\sigma^2}} \end{aligned}$$

Hence,  $\Delta d \sim \mathcal{N}(0; \sigma)$ .

QED

Normalizing the vector in Equation (3) to range (0, 1] by timing a constant scalar  $\frac{(\sqrt{2\pi}\sigma)^{\frac{1}{2}}}{\Delta x}$ , we get our positional encoding. In practice,  $\sigma$  can be a hyperparameter or a learned parameter of a model.

### 3.5. Auxiliary Occupancy Supervision with True Negatives

Occupancy map is 3D voxels in form of a 3D matrix of which each element indicates whether a voxel is occupied

by any objects. Inspired by PLUMENet [34], our model estimates the occupancy map as an auxiliary target to avoid overfitting with tighter constraints. To produce ground truth for the occupancy map, one way is to take voxels containing lidar points as positive samples and voxels without points as empty space. While all positive samples are guaranteed to be true, voxels occupied by an object but not visible to lidar will be false negative samples (see Figure 4a). To fix this problem, only voxels passed through by laser beams and without lidar points are chosen as negative samples as Figure 4b. Though the constrain is looser having fewer negative samples, it can produce labels without false positives and false negatives.

### 3.6. Multi-task Heads

For 3D detection head, we deploy settings from the Single Shot Detector(SSD) [14] and assign ground truth to axis-aligned anchor boxes using 2D Intersection over Union (IoU) [3] following PointPillars [10]. Parallel to the detection head, we use the PLUMENet [34] setup to predict the occupancy map.

## 4. Experiments

### 4.1. KITTI Object Detection Dataset

KITTI is a pioneer dataset for visual recognition systems in robotic applications [4]. The data is captured from a VW station wagon equipped with four video cameras

Method	3D AP@0.7			3D AP@0.5		
	Easy	Mod.	Hard	Easy	Mod.	Hard
Sinusoidal*	16.26	12.73	10.44	56.91	40.52	33.49
Learned*	21.47	14.44	11.34	64.69	45.13	37.61
Gaussian*	20.25	14.58	11.94	58.91	41.32	34.04
Gaussian	23.40	15.55	12.85	65.02	44.69	36.64

Table 2. Ablation experiments for positional encodings. On par with the learned method in performance, our encoding function has the advantage of encoding continuous values. \*Sigmoid activation is applied. Our gaussian positional encoding is superior to the sinusoidal method to a large extent.

Method	3D AP@0.7			3D AP@0.5		
	Easy	Mod.	Hard	Easy	Mod.	Hard
Projection	5.35	3.49	2.8	35.45	23.68	19.94
Transformer	1.98	1.43	1.20	28.68	18.26	15.71
LRA	23.40	15.55	12.85	65.02	44.69	36.64

Table 3. Ablation experiments for choices of transforming 2D features to 3D space. Constrained by GPU memory, we use a fast transformer, Nystromformer [36]. "LRA" indicates local ray attention.

Method	3D AP@0.7			3D AP@0.5		
	Easy	Mod.	Hard	Easy	Mod.	Hard
Baseline	23.40	15.55	12.85	65.02	44.69	36.64
+AUG	23.12	15.23	12.55	65.59	45.15	38.25
+AUG+OAB	38.25	27.60	23.48	78.95	63.16	56.09

Table 4. Ablation experiments for the orientation-aware backbone. "AUG" indicates random global rotation augmentation. "OAB" represents an orientation-aware backbone. OAB is a necessity for AUG to boost model performance.

(1392×512 pixels), a Velodyne 64-beam laser scanner, and a localization unit. 7481 training samples and 7518 testing samples are provided, each of which contains two color images, two grayscale images, a point cloud, object annotations in form of 3D bounding boxes, and a calibration file. Only annotations of the training set are made public. A total of 80256 labeled objects are divided into 7 classes: 'Car', 'Van', 'Truck', 'Pedestrian', 'Person (sitting)', 'Cyclist', 'Tram' and 'Misc'. There are 3 difficulty levels, easy, moderate, and hard, defined by bounding box height and occlusion level. The 3D object detection benchmark ranks all methods using the average precision of precision-recall curves with 40 recall positions.

Method	3D AP@0.7			3D AP@0.5		
	Easy	Mod.	Hard	Easy	Mod.	Hard
Baseline	21.55	14.84	11.94	60.08	42.06	35.48
w/ TN label	23.40	15.55	12.85	65.02	44.69	36.64

Table 5. Ablation experiments for occupancy supervision. All empty voxels are negative samples in the baseline while only those passed through by lidar beams are assigned negative for "w/ TN label".

## 4.2. Implementation Details

The 2D backbone is DD3D [20] pretrained V2-99 [11] on DDAD15M [5] for depth estimation. The BEV backbone is 3D-BEV network in PLUMENet-Small [34].

For evaluation on the KITTI test server, we trained on the training set. While for the ablation study, we trained on the subset of the training set the same as SECOND [37]. All models are trained 80 epochs using AdamW [17] optimizer with a one-cycle learning rate scheduler [29]. The maximum learning rate is set to 0.0003 and the dividing factor is 20.

For data augmentation, we randomly select an image captured by a left or right color camera for each sample; we deploy random flipping of images and random rotation as described in Sec. 3.3.

## 4.3. Benchmark Evaluation

To do a horizontal comparison of monocular models, we evaluate our result of the test set on the KITTI server. The results are summarized in Table 1. On the KITTI 3D object detection benchmark, our model ranks first in all difficulty levels among all of the previously monocular models by achieving an AP moderate score of 20.95%. Our model outperforms the previously best 3D intermediate representation method [7] by a large margin of 3.15%. On the KITTI bird's eye view benchmark, our model achieves an AP moderate score of 28.50%, outperforming all of the previously published models.

## 4.4. Ablation Study

To demonstrate the importance of each component of our model, we measure the change in average precision evaluated on the KITTI validation set while varying our model.

### 4.4.1 Positional Encodings

In Table 2, we replace gaussian positional encodings with sinusoidal [31] and learned positional encodings. We do not apply random world rotation to any of our models because this would make the distance from each voxel to the image plane vary greatly, which would require a continuous positional encoding function instead of a discrete learned

Method	3D AP@0.7			BEV AP@0.7			3D AP@0.5			BEV AP@0.5		
	Easy	Mod.	Hard	Easy	Mod.	Hard	Easy	Mod.	Hard	Easy	Mod.	Hard
-Occu. with TN	34.59	24.74	21.08	45.13	32.90	28.50	74.96	58.92	52.03	78.79	64.03	56.95
-Local Ray Att.	37.09	26.96	22.94	47.81	34.92	30.38	75.44	60.17	53.17	78.78	65.29	58.99
-Orientation-Aware	23.28	15.58	12.89	34.44	23.35	19.39	65.19	44.52	36.80	69.88	48.42	41.96
Full Model	38.25	27.60	23.48	49.58	36.05	31.26	78.95	63.16	56.09	81.76	66.42	60.43

Table 6. Ablation experiments for key contributions.

function. Both learned and gaussian positional encoding significantly surpass the sinusoidal way. While gaussian and learned ways obtain similar performance taking all the metrics into account, the gaussian encoding prevails over learned encoding in its ability to represent continuous value rather than a fixed amount of discrete values.

#### 4.4.2 Local Ray Attention Mechanism

To verify the effectiveness of the local ray attention mechanism, we vary the 2d-3d transformation components as in Figure 2. Random world rotation is not applied. We observe that removing local ray attention hurts model quality considerably. Although the pure transformer method fit training samples well, it suffers from severe overfitting such that it is even worse than direct projection.

#### 4.4.3 Orientation-Aware 2D Image Backbone

In Table 4, we observe that simply applying global rotation of the ego car coordinate brings hardly any gain of AP. The baseline model is a reduced model without random world rotation augmentation and orientation-aware backbone. With an orientation-aware backbone, the result is improved remarkably to the extent of 15.13%. This suggests that ensuring implicit and explicit features to be consistent is vital in transforming 2D features into 3D space.

#### 4.4.4 Occupancy Supervision with True Negative

Additionally, we experimented with the two label assignment methods of the occupancy map. The baseline uses the label assignment scheme as Figure 4a. As expected, though occupancy map with true negative marks fewer voxels resulting in looser supervision, it is very helpful in avoiding over-fitting by providing more correct samples (see Table 5).

#### 4.4.5 Key Contributions

We also do ablation studies to verify the value of our key contributions. As Table 6 illustrated, removing any of these components impairs the performance of the model.

## 5. Conclusion

In this work, we identify inconsistency of implicit and explicit features as the primary obstacle that hinders the development of methods using intermedia 3D representation. Based on this insight, we propose **CIEF** with orientation-aware image backbone, local ray attention mechanism, and handcrafted gaussian encoding. Extensive ablation experiments show that ensuring the consistency significantly improves the performance of our model. The local ray attention mechanism and gaussian encoding have proven to be effective as expected. Overall, **CIEF** put a spurt on detection accuracy in KITTI 3D and BEV benchmark showing promising results.

## References

- [1] Yongjian Chen, Lei Tai, Kai Sun, and Mingyang Li. Monopair: Monocular 3d object detection using pairwise spatial relationships. In *2020 IEEE/CVF Conference on Computer Vision and Pattern Recognition (CVPR)*, pages 12090–12099, 2020. 2
- [2] Zihang Dai, Zhilin Yang, Yiming Yang, Jaime Carbonell, Quoc Le, and Ruslan Salakhutdinov. Transformer-XL: Attentive language models beyond a fixed-length context. In *Proceedings of the 57th Annual Meeting of the Association for Computational Linguistics*, pages 2978–2988, Florence, Italy, July 2019. Association for Computational Linguistics. 4
- [3] Mark Everingham, Luc Van Gool, Christopher K. I. Williams, John M. Winn, and Andrew Zisserman. The pascal visual object classes (voc) challenge. *International Journal of Computer Vision*, 88:303–338, 2009. 5
- [4] Andreas Geiger, Philip Lenz, and Raquel Urtasun. Are we ready for autonomous driving? the kitti vision benchmark suite. *2012 IEEE Conference on Computer Vision and Pattern Recognition*, pages 3354–3361, 2012. 5
- [5] Vitor Campanholo Guizilini, Rares Ambrus, Sudeep Pillai, and Adrien Gaidon. 3d packing for self-supervised monocular depth estimation. *2020 IEEE/CVF Conference on Computer Vision and Pattern Recognition (CVPR)*, pages 2482–2491, 2020. 6
- [6] Muhamad Amirul Haq, Shanq-Jang Ruan, Mei-En Shao, Qazi Mazhar ul Haq, Pei-Jung Liang, and De-Qin Gao. One stage monocular 3d object detection utilizing discrete depth

- and orientation representation. *IEEE Transactions on Intelligent Transportation Systems*, 2022. 5
- [7] Henan Hu, Ming Zhu, Muyu Li, and Kwok-Leung Chan. Deep learning-based monocular 3d object detection with refinement of depth information. *Sensors (Basel, Switzerland)*, 22, 2022. 5, 6
- [8] Junjie Huang, Guan Huang, Zheng Zhu, and Dalong Du. Bevdet: High-performance multi-camera 3d object detection in bird-eye-view. *ArXiv*, abs/2112.11790, 2021. 3, 4
- [9] Kuan-Chih Huang, Tsung-Han Wu, Hung-Ting Su, and Winston H. Hsu. Monodtr: Monocular 3d object detection with depth-aware transformer. *ArXiv*, abs/2203.10981, 2022. 2, 5
- [10] Alex H. Lang, Sourabh Vora, Holger Caesar, Lubing Zhou, Jiong Yang, and Oscar Beijbom. Pointpillars: Fast encoders for object detection from point clouds. *2019 IEEE/CVF Conference on Computer Vision and Pattern Recognition (CVPR)*, pages 12689–12697, 2019. 5
- [11] Youngwan Lee and Jongyoul Park. Centermask: Real-time anchor-free instance segmentation. *2020 IEEE/CVF Conference on Computer Vision and Pattern Recognition (CVPR)*, pages 13903–13912, 2020. 6
- [12] Zhuoling Li, Z. Qu, Yang Zhou, Jianzhuang Liu, Haoqian Wang, and Lihui Jiang. Diversity matters: Fully exploiting depth clues for reliable monocular 3d object detection. *ArXiv*, abs/2205.09373, 2022. 2, 5
- [13] Zhiqi Li, Wenhai Wang, Hongyang Li, Enze Xie, Chonghao Sima, Tong Lu, Yu Qiao, and Jifeng Dai. Bevformer: Learning bird’s-eye-view representation from multi-camera images via spatiotemporal transformers. *arXiv preprint arXiv:2203.17270*, 2022. 3
- [14] W. Liu, Dragomir Anguelov, D. Erhan, Christian Szegedy, Scott E. Reed, Cheng-Yang Fu, and Alexander C. Berg. Ssd: Single shot multibox detector. In *ECCV*, 2016. 5
- [15] Xianpeng Liu, Nan Xue, and Tianfu Wu. Learning auxiliary monocular contexts helps monocular 3d object detection. *ArXiv*, abs/2112.04628, 2021. 2, 5
- [16] Zechen Liu, Zizhang Wu, and Roland Tóth. SMOKE: Single-stage monocular 3d object detection via keypoint estimation. *arXiv preprint arXiv:2002.10111*, 2020. 2
- [17] Ilya Loshchilov and Frank Hutter. Decoupled weight decay regularization. In *ICLR*, 2019. 6
- [18] Xinzhu Ma, Zihui Wang, Haojie Li, Pengbo Zhang, Wanli Ouyang, and Xin Fan. Accurate monocular 3d object detection via color-embedded 3d reconstruction for autonomous driving. In *Proceedings of the IEEE/CVF International Conference on Computer Vision*, pages 6851–6860, 2019. 1, 3, 5
- [19] Yi nan Chen, Hang Dai, and Yong Ding. Pseudo-stereo for monocular 3d object detection in autonomous driving. *ArXiv*, abs/2203.02112, 2022. 2, 5
- [20] Dennis Park, Rares Ambrus, Vitor Campanholo Guizilini, Jie Li, and Adrien Gaidon. Is pseudo-lidar needed for monocular 3d object detection? *2021 IEEE/CVF International Conference on Computer Vision (ICCV)*, pages 3122–3132, 2021. 2, 5, 6
- [21] Liang Peng, Fei Liu, Zhengxu Yu, Senbo Yan, Dan Deng, and Deng Cai. Lidar point cloud guided monocular 3d object detection. *ArXiv*, abs/2104.09035, 2021. 3, 5
- [22] Liang Peng, Senbo Yan, Chenxi Huang, Xiaofei He, and Deng Cai. Digging into output representation for monocular 3d object detection, 2022. 5
- [23] Jonah Philion and Sanja Fidler. Lift, splat, shoot: Encoding images from arbitrary camera rigs by implicitly unprojecting to 3d. In Andrea Vedaldi, Horst Bischof, Thomas Brox, and Jan-Michael Frahm, editors, *Computer Vision – ECCV 2020*, pages 194–210, Cham, 2020. Springer International Publishing. 1, 3
- [24] Charles R Qi, Hao Su, Kaichun Mo, and Leonidas J Guibas. Pointnet: Deep learning on point sets for 3d classification and segmentation. In *Proceedings of the IEEE conference on computer vision and pattern recognition*, pages 652–660, 2017. 2
- [25] Colin Raffel, Noam Shazeer, Adam Roberts, Katherine Lee, Sharan Narang, Michael Matena, Yanqi Zhou, Wei Li, and Peter J. Liu. Exploring the limits of transfer learning with a unified text-to-text transformer. *Journal of Machine Learning Research*, 21(140):1–67, 2020. 4
- [26] Cody Reading, Ali Harakeh, Julia Chae, and Steven L Waslander. Categorical depth distribution network for monocular 3d object detection. In *Proceedings of the IEEE/CVF Conference on Computer Vision and Pattern Recognition*, pages 8555–8564, 2021. 1, 3, 5
- [27] Thomas Roddick, Alex Kendall, and Roberto Cipolla. Orthographic feature transform for monocular 3d object detection. In Kirill Sidorov and Yulia Hicks, editors, *Proceedings of the British Machine Vision Conference (BMVC)*, pages 59.1–59.13. BMVA Press, September 2019. 1, 3, 5
- [28] Andrea Simonelli, Samuel Rota Buló, Lorenzo Porzi, Manuel Lopez-Antequera, and Peter Kontschieder. Disentangling monocular 3d object detection. In *Proceedings of the IEEE/CVF International Conference on Computer Vision (ICCV)*, October 2019. 5
- [29] Leslie N. Smith and Nicholay Topin. Super-convergence: very fast training of neural networks using large learning rates. In *Defense + Commercial Sensing*, 2019. 6
- [30] Zhi Tian, Chunhua Shen, Hao Chen, and Tong He. FCOS: Fully convolutional one-stage object detection. In *Proc. Int. Conf. Computer Vision (ICCV)*, 2019. 2
- [31] Ashish Vaswani, Noam Shazeer, Niki Parmar, Jakob Uszkoreit, Llion Jones, Aidan N Gomez, Łukasz Kaiser, and Illia Polosukhin. Attention is all you need. In I. Guyon, U. Von Luxburg, S. Bengio, H. Wallach, R. Fergus, S. Vishwanathan, and R. Garnett, editors, *Advances in Neural Information Processing Systems*, volume 30. Curran Associates, Inc., 2017. 6
- [32] Tai Wang, Xinge Zhu, Jiangmiao Pang, and Dahua Lin. FCOS3D: Fully convolutional one-stage monocular 3d object detection. In *Proceedings of the IEEE/CVF International Conference on Computer Vision (ICCV) Workshops*, 2021. 2
- [33] Yue Wang, Vitor Guizilini, Tianyuan Zhang, Yilun Wang, Hang Zhao, , and Justin M. Solomon. Detr3d: 3d object detection from multi-view images via 3d-to-2d queries. In *The Conference on Robot Learning (CoRL)*, 2021. 2
- [34] Yan Wang, Binh Yang, Rui Hu, Ming Liang, and Raquel Urtasun. Plumenet: Efficient 3d object detection from stereo

- images. *2021 IEEE/RSJ International Conference on Intelligent Robots and Systems (IROS)*, pages 3383–3390, 2021. 5, 6
- [35] Xinshuo Weng and Kris Kitani. Monocular 3d object detection with pseudo-lidar point cloud. In *Proceedings of the IEEE/CVF International Conference on Computer Vision Workshops*, pages 0–0, 2019. 1, 3
- [36] Yunyang Xiong, Zhanpeng Zeng, Rudrasis Chakraborty, Mingxing Tan, Glenn M. Fung, Yin Li, and Vikas Singh. Nyströmformer: A nyström-based algorithm for approximating self-attention. *Proceedings of the ... AAAI Conference on Artificial Intelligence. AAAI Conference on Artificial Intelligence*, 35 16:14138–14148, 2021. 6
- [37] Yan Yan, Yuxing Mao, and Bo Li. Second: Sparsely embedded convolutional detection. *Sensors*, 18(10):3337, 2018. 1, 4, 6
- [38] Renrui Zhang, Hang Qiu, Tai Wang, Xuan Xu, Ziyu Guo, Yu Jiao Qiao, Peng Gao, and Hongsheng Li. Monodetr: Depth-aware transformer for monocular 3d object detection. *ArXiv*, abs/2203.13310, 2022. 5
- [39] Xingyi Zhou, Dequan Wang, and Philipp Krähenbühl. Objects as points. In *arXiv preprint arXiv:1904.07850*, 2019. 2